

### **ICPES 2025**

40<sup>th</sup> INTERNATIONAL CONFERENCE ON PRODUCTION ENGINEERING - SERBIA 2025

DOI: <u>10.46793/ICPES25.072G</u>



University of Nis
Faculty of Mechanical
Engineering

Nis, Serbia, 18 - 19th September 2025

# ELECTROMAGNETIC FIELD ANALYSIS AND PREDICTIVE MODELING IN FIBER LASER CUTTING OF REFRACTORY STEELS

Constantin CRISTINEL GIRDU<sup>1</sup>, Miloš MADIĆ<sup>2</sup>, Catalin GHEORGHE<sup>3\*</sup>,
Daniel LATES<sup>4</sup>, Bogdan CĂTĂLIN IACOB<sup>5</sup>

Orcid: 0000-0002-4653-6957; Orcid: 0000-0002-2310-2590; Orcid: 0000-0003-4090-1439, 

<sup>1</sup>Department of Manufacturing Engineering, Transilvania University of Brasov, Eroilor Street 29, 
500036 Brasov, Romania

<sup>2</sup>Faculty of Mechanical Engineering, University of Niš, A. Medvedeva 14, 18000 Niš, Serbia <sup>3</sup>Department of Engineering and Industrial Management, Transilvania University of Brasov, Eroilor Street 29, 500036 Brasov, Romania

<sup>4</sup>IRUM SA, Axente Sever 6, 545300 Reghin, Romania <sup>5</sup>Oltenia Energy Complex SA, Alexandru Ioan Cuza 5, 210140 Targu-Jiu, Romania \*Corresponding author: gheorghe.c@unitbv.ro

**Abstract:** This study presents a theoretical and experimental framework for modelling the electromagnetic field generated by a high-power fiber laser beam and for predicting the hardness variations in refractory steels subjected to laser cutting. Based on Maxwell's equations, a mathematical model is developed to describe the propagation of electric and magnetic fields in space and time, linking beam parameters, such as power, focal position, and cutting speed, with the physical characteristics of laser radiation. This theoretical foundation is applied to analyse the behaviour of an X10AlCr180 alloy, commonly used in high-temperature industrial applications. Changes in hardness within the heat-affected zone after oxygen-assisted laser cutting are investigated. Experimental data are statistically processed, and a quasi-linear predictive model is developed, achieving a determination coefficient R<sup>2</sup>= 99.52%. The results indicate that laser power and focal position have the most significant influence on hardness. This work highlights the relevance of integrating electromagnetic wave theory with thermal-material interactions in advanced manufacturing processes.

**Keywords:** fiber laser cutting; electromagnetic field modelling; refractory steels; hardness.

#### 1. INTRODUCTION

High-power laser cutting is one of the most advanced methods for processing metallic materials, highly valued for its precision, speed, and adaptability to challenging materials such as refractory steels. Controlling the surface quality and post-cutting mechanical properties is essential in critical industrial applications, such as steam boiler components or energy system installations.

In this context, the alloyed steel X10AlCr180 is frequently used due to its excellent resistance to high temperatures and corrosion. However, its behaviour during laser cutting presents challenges related to

microstructural changes and the reduction of hardness in the heat-affected zone (HAZ). Several studies have shown that the choice of technological parameters, such as laser power, cutting speed, and focal position, directly influences the mechanical characteristics of the processed surfaces [1], [2].

To optimize the cutting process, recent research has employed methods such as statistical modeling using RSM (Response Surface Methodology) [3], intelligence algorithms [4], or multi-objective optimization techniques [5]. Nevertheless, few studies address the phenomenon from a fundamental perspective, starting with the modelling of electromagnetic propagation generated by the laser beam, based on Maxwell's equations [6]. For instance, Turkkan et al. (2023) applied a multiobjective optimization using Taguchi methods and Grey Relational Analysis for laser cutting of AISI 304L stainless steel, identifying duty cycle and frequency as the most influential parameters for reducing roughness and kerf width [7].

This study proposes an integrated theoretical-experimental approach, combining mathematical modelling of the electromagnetic field generated by the laser beam with the analysis of the hardness of X10AlCr180 steel after fiber laser cutting. Quasi-linear predictive equations for hardness are formulated and empirically validated based on a factorial experimental design with eight processing variants, using a BySmart Fiber Bystronic laser cutting machine. The correlation of theoretical and experimental results provides a comprehensive view of the influence of cutting parameters on the material's hardness, thus contributing to the optimization of the process applied to advanced steels. According to Pimenov et al. (2023), heat-resistant steels with complex structures and high alloying element content (Cr, Ni, Al) are considered difficult-to-machine materials, requiring the use of advanced technologies such as high-precision laser

cutting [8].

#### 2. LITERATURE REVIEW

## 2.1. Optimization of technological parameters in laser cutting

Fiber laser cutting has gained significant traction in the processing of advanced materials due to its ability to deliver high-precision cuts, minimized HAZ, and precise control over microstructural changes. Numerous studies have highlighted the direct influence of technological parameters, particularly laser power, cutting speed, and focal position, on local hardness, surface topography, and mechanical behaviour of the processed material [9].

Research on structural steels has shown that varying these parameters can significantly alter the hardness within the heat-affected zone. For example, Safari et al. demonstrated that in Hardox 400 steel, process optimization can be effectively achieved using robust statistical models that reveal the sensitivity of HAZ hardness to changes in process parameters [1]. Similarly, al. combined Yurdakul et the **RSM** methodology with the Analytic Hierarchy Process, resulting in an efficient multicriteria framework for optimizing the cutting of St-52 steel [2].

Advancements in artificial intelligence have introduced new tools for modelling the complex relationships within the cutting process. Sket et al. implemented neural networks to predict thermal and geometric behaviour in stainless steels, achieving better performance than traditional regression models [3]. Other approaches focused on improving experimental data distribution through methods like Latin Hypercube Sampling, contributing to more effective calibration of predictive models [4].

For difficult to cut materials such as 904L super-austenitic steel, Balasubramaniyan and Rajkumar (2025) showed that simultaneous optimization of laser power, feed rate, and

pulse frequency led to higher material removal rates and improved surface hardness, highlighting the effects of the resolidified layer [10]. In a recent review, Alsaadawy et al. (2024) reported that using low laser power combined with high cutting speed, moderate assist gas pressure, and nitrogen gas significantly reduced machining defects, including excessive roughness and burr formation [11].

Basak et al. (2025) analyzed the impact of intrinsic material properties on surface quality, concluding that these can have a greater influence than process parameters [12]. In their study, hardness decreased by up to 22.7% in SS316 stainless steel, suggesting a strong dependence of thermomechanical response on material composition. Additionally, Mahrle et al. (2021), through a factorial experimental design, identified a significant correlation between cut edge roughness and kerf geometry, emphasizing that internal process parameters may outweigh external factors such as assist gas pressure [13].

Overall, the literature shows a continuous effort to identify optimal configurations of technological parameters to improve the quality of laser-cut surfaces. However, most studies focus on empirical or statistical and tend to overlook approaches fundamental perspective based on modelling the electromagnetic field generated by the laser beam. This gap underscores the need for a combined approach that links process parameters with the behaviour electromagnetic waves, enabling a deeper understanding of the interaction between the laser beam and the material.

#### 2.2 Theoretical modelling of laser beam propagation

A central objective of this research is the formulation of a rigorous theoretical model of the electromagnetic field generated by the laser beam during the cutting process. To achieve this, the starting point is the

fundamental equations of electromagnetism developed by James Clerk Maxwell, which describe how electromagnetic waves are generated and propagate in a vacuum. The laser beam is interpreted as a plane electromagnetic wave, composed synchronized oscillations of the electric and magnetic fields, propagating at the speed of light ccc.

According to classical theory, a timevarying electric field induces a time-varying magnetic field, and this reciprocal process gives rise to the propagation of electromagnetic wave. Maxwell's equations, in their differential form for vacuum conditions, are expressed as follows:

$$rotH=\nabla\times H=\frac{\partial D}{\partial t}$$
 (1)  
$$rotE=\nabla\times E=-\frac{\partial B}{\partial t}$$
 (2)

$$rotE = \nabla \times E = -\frac{\partial B}{\partial t}$$
 (2)

$$divD = \nabla \cdot D = 0 \tag{3}$$

$$divB = \nabla \cdot B = 0 \tag{4}$$

We start from the equation involving differential operators i:

$$\nabla \times (\nabla \times H) = \nabla \cdot (\nabla \cdot H) - \Delta H \tag{5}$$

in which E is the electric field intensity, D the electric displacement field, H the magnetic field intensity, and B the magnetic flux density.

$$D=\varepsilon_0\cdot E, B=\mu_0\cdot H \tag{6}$$

These relations are combined, resulting in:

$$\nabla \times \frac{\partial D}{\partial t} = \nabla \cdot (\nabla \cdot H) - \Delta H \tag{7}$$
 For a stationary field:  $\nabla \cdot H = 0$ 

$$\Delta H + \nabla \times \frac{\partial D}{\partial t} = 0$$
 (8)

$$\Delta H + \nabla \times \frac{\partial D}{\partial t} = 0$$
 (8)  
 
$$\Delta H + \nabla \times \varepsilon_0 \frac{\partial E}{\partial t} = 0$$
 (9)

$$\Delta H + \varepsilon_0 \frac{\partial}{\partial t} (\nabla \times E) = 0$$
 (10)

$$\Delta H + \varepsilon_0 \frac{\partial}{\partial t} (\nabla \times E) = 0$$
 (10)  
$$\Delta H + \varepsilon_0 \frac{\partial}{\partial t} (-\frac{\partial B}{\partial t}) = 0$$
 (11)

$$\Delta H - \varepsilon_0 \frac{\partial^2 B}{\partial t^2} = 0 \tag{12}$$

$$\Delta H - \varepsilon_0 \mu_0 \frac{\partial^2 H}{\partial t^2} = 0 \tag{13}$$

In Cartesian coordinates, the equation becomes:

$$\frac{\partial^{2}H}{\partial x^{2}} + \frac{\partial^{2}H}{\partial y^{2}} + \frac{\partial^{2}H}{\partial z^{2}} - \varepsilon_{0}\mu_{0}\frac{\partial^{2}H}{\partial t^{2}} = 0$$
 (14)

$$\frac{\partial^2 H}{\partial x^2} + \frac{\partial^2 H}{\partial y^2} + \frac{\partial^2 H}{\partial z^2} - \frac{1}{c^2} \frac{\partial^2 H}{\partial t^2} = 0$$
 (15)

The solution of the second-order differential

equation:

$$H=H_0\cos(\omega t-kz)$$
 (16)

where  $H_0$  is the magnetic amplitude,  $\omega$  is the angular frequency, k is the wave number, and z is the direction of laser wave propagation.

At the origin of the axes, where the laser source is located, electromagnetic waves are generated with the following components:

$$H=H_0\cos(\omega t) \tag{17}$$

$$E=E_0\cos(\omega t) \tag{18}$$

At a distance z from the origin of the Cartesian system, the following waves of the coupled fields are generated:

$$H=H_0\cos(\omega t-kz)$$
 (19)

$$E=E_0\cos(\omega t-kz) \tag{20}$$

Based on previous relations we can develop the field equation:

$$H=H_0\cos\left(\frac{2\pi}{T}t-\frac{2\pi}{\lambda}z\right)=H_0\cos(2\pi(\frac{t}{T}-\frac{z}{\lambda}))$$
 (21)

The relationship between the electric field and the magnetic field is governed by the principle of cause and effect, where one acts as the cause and the other as the effect, resulting in the propagation of laser light. These fields are in phase and simultaneously reach their maximum and minimum values. An important relation can be obtained by setting the phase as:

$$\phi = \omega t - kz$$
 (22)

When we apply Fermat's theorem to the phase of the wave, we obtain an extremum point:

$$\frac{\partial \Phi}{\partial t} = 0 \tag{23}$$

$$c = \frac{\partial z}{\partial t} = \frac{\omega}{t} = \frac{\lambda}{T}$$
 (24)

When the wavelength of electromagnetic radiation is very short, the oscillation period of the associated field becomes extremely brief. Lasers operating in the ultraviolet region the electromagnetic spectrum characterized by short oscillation periods and high electric field amplitudes, which grant them a high energy density. The intensity of laser radiation is directly influenced by the rapid temporal variation of the electric and magnetic fields, and the synchronization of these fields in space and time leads to the formation of a high-energy coherent beam. The electric field plays a crucial role in the

spatial displacement of the magnetic field lines, while the magnetic field loops around the beam in a circular manner, thereby defining the geometry of the laser beam.

This mutual interaction leads to the generation of a collimated beam, directed along the longitudinal axis (the Oz direction), which propagates at the speed of light in a vacuum. The electric field oscillates in a plane perpendicular to the direction of propagation (along the Ox axis), while the magnetic field oscillates perpendicular to it (along the Oy direction), the two being orthogonal both to each other and to the propagation direction. From a physical standpoint, the electric field can be interpreted as a magnetic moment generated by the cross product between the speed of light and the magnetic field intensity, according to the relation:

E=c X B=c X 
$$\mu_0$$
H= $\mu_0$ (c X H) (25)

Depending on the values of E and B (or H), laser light is concentrated into a very small diameter and is characterized by different wavelengths. The laser light spectrum spans the infrared, visible, and ultraviolet regions. The amplitude of the electric field is much greater than that of the magnetic field, by a factor of c (speed of light).

$$E_0 = c \times B_0$$
 (26)

The greater the value of E<sub>0</sub>, the higher the frequency of the laser light, which gives rise to high-power lasers possessing strong electric fields of significant magnitude. When the amplitudes E<sub>0</sub> and B<sub>0</sub> increase, this results in a strong concentration of laser light in a small space, with higher luminous excitation and intensity. The circular cross-section of the beam is primarily due to the magnetic field. This flash, sometimes of different colours or invisible, is generated by a laser light source with beam directionality confined to a narrow parallel path. The wavelength is the same for both the electric and magnetic fields. When the wavelength drops below 1 nm, it is observed that the energy of the flash increases while the distance between two field maxima decreases.

When laser radiation interacts with matter, collisions occur between laser photons and electrons, as well as between laser photons and ions, resulting in physical phenomena such as absorption and reflection. The laser energy density is defined as the amount of light energy per unit volume:

$$w = \frac{E}{V} = \frac{Nh\vartheta}{V} = nh\vartheta \tag{27}$$

Taking into account the field laws, the energy density is expressed as follows:

$$w=\varepsilon_0\cdot E^2$$
 (28)

The maximum energy density is obtained when the amplitudes of the electric and magnetic fields reach their peak values and are in perfect phase synchronization  $cos(\omega t-kz)=1$ ,

$$\mathbf{w}_{\mathsf{m}} = \boldsymbol{\varepsilon}_{\mathsf{0}} \cdot \mathbf{E}_{\mathsf{0}}^{2} = \boldsymbol{\varepsilon}_{\mathsf{0}} \cdot \mathbf{I}_{\mathsf{0}} \tag{29}$$

Incident laser intensity is:

$$I_0 = \frac{4P}{\pi \cdot d^2} = E_0^2 \tag{30}$$

We can calculate the amplitude E of the radiation field:

$$E_0 = \left(\frac{4P}{\pi \cdot d^2}\right)^{1/2} \tag{31}$$

where P is the laser power, and d is the spot diameter, an important parameter of the laser light field. In vacuum, the electric field quantifies the magnetic field by the value of c. Based on the operating parameters of the laser, we can calculate the maximum value of the electric field.

#### 3. MATERIAL AND DESIGN OF EXPERIMENTS

#### 3.1 Material

The material analysed in this study is a sheet of alloy steel of type X10AlCr180, characterized by a high content of chromium (approximately 18%), aluminium, and silicon. This alloy is intended for use under extreme temperature and corrosion conditions and is commonly used in the construction of reinforcements and support elements for the refractory linings of pulverized coal burners in boilers used for generating superheated steam. The initial hardness of the sheet, determined using the Vickers method, falls within the range of 220–280 HV, which is

typical for refractory materials with high thermal stability.

#### 3.2 Experimental setup

The cutting experiments were carried out using a fiber laser with a maximum radiation power of P = 5200 W and a focused spot with a diameter of d = 0.38 mm, within which a maximum electric field intensity of  $E_0 = 2.17 \times$ 10<sup>5</sup> V/m was achieved. Following interaction with the material, this electric instantaneously generates, through relativistic effects, a magnetic induction field of  $B_0 = 0.7 \times 10^{-3}$  T. The energy delivered by the laser beam heats, melts, and vaporizes the surface of the metallic target, and collisions with atomic electrons result in excitations and ionizations, also producing intense luminous effects.

Theoretical modelling of the electromagnetic field propagation, based on specific operating parameters, enables a detailed understanding of energy transfer and the effects induced in the material. This approach allows the correlation of field distribution with the microstructural and mechanical changes that occur after cutting.



**Figure 1.** BySmart Fiber Bystronic laser cutting machine used in the experiments.

The tests were conducted using the BySmart Fiber Bystronic equipment designed for high-precision processing. It enables fine, clean cuts with high tolerances and virtually no burr formation, eliminating, in most cases, the need for subsequent machining. Its noncontact operation ensures minimal wear of

components and significantly reduces technological losses. The image of the equipment used is shown in Figure 1.

For a comparative evaluation of performance, the results obtained with the conventional Zinser 2325 equipment, based on oxy-gas cutting, were also analysed. This machine, shown in Figure 2, is significantly slower, involves direct contact with the material, and often produces burrs and thermal deformations, requiring additional processing (grinding, deburring).



**Figure 2.** Zinser 2325 cutting machine used for performance evaluation comparison

An essential advantage of laser technology is the minimal material loss, due to the extremely thin beam that produces narrow cutting kerfs. This enables optimized nesting of parts on the sheet, contributing to process efficiency and cost reduction. Moreover, the absence of mechanical contact eliminates tool wear, an important benefit compared to conventional machining methods.

#### 3.3 Experimental design

Hardness was selected as the main evaluation criterion for assessing the quality of parts obtained through oxygen-assisted laser cutting, given its direct impact on mechanical performance in critical applications. Due to the unstable behavior of the material in its molten state, conventional oxy-fuel cutting does not allow for clean and precise edges. This is why laser technology

was chosen, as it offers superior accuracy and minimal material loss by narrowing the cutting kerf.

To quantify the efficiency of the process, a removal index (I<sub>s</sub>) was introduced, defined as the ratio between the amount of usable material remaining in the part and the total amount of material cut:

 $I_s = \frac{\text{Amount of cut material remaining in the part}}{\text{Total amount of material cut}}$ 

An index close to 1 reflects an efficient cutting process, with high precision and minimal losses, essential characteristics for high-performance industrial machining. The novelty of this research lies in the detailed experimental analysis of surface hardness on parts cut with high-power fiber laser, correlated with microstructural changes induced in the HAZ.

Hardness measurements were performed using a portable KrautKramer MIC 10 hardness tester equipped with a diamond-tipped probe, as illustrated in Figure 3. The recorded values showed a slight decrease in hardness within the HAZ, a phenomenon attributed to annealing and local softening effects. These changes are associated with the migration of alloying atoms (Cr, Al, Si), increased interatomic distances, and reduced bonding forces, processes induced by the high thermal concentration generated by the laser beam.

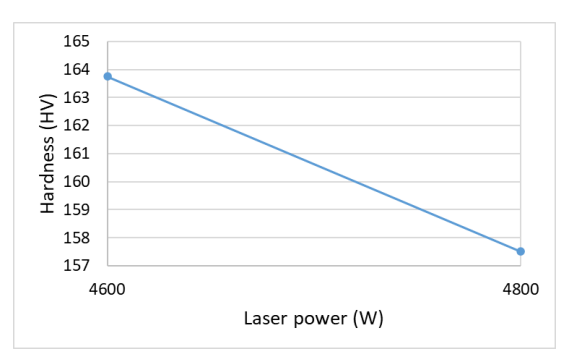


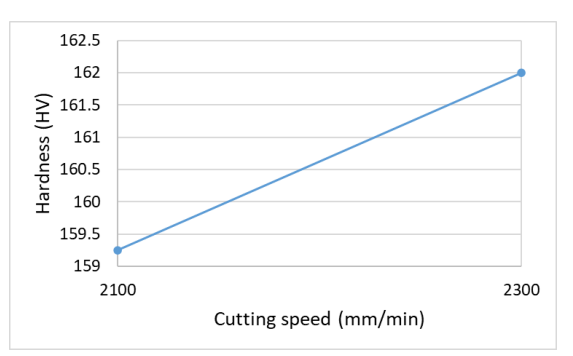
**Figure 3.** Portable KrautKramer MIC 10 device used for hardness measurement.

The average hardness obtained after cutting was approximately 150 HV, which is

lower compared to the initial values of the raw material. For the experimental design, a 2<sup>3</sup> factorial matrix was applied, from which 8 relevant experimental points (out of a possible 27) were analysed, as shown in Table 1. Based on these data, the main and interaction effects of the independent variables (laser power, cutting speed, focal position) were estimated, and the resulting statistical model allows for the prediction of hardness values.

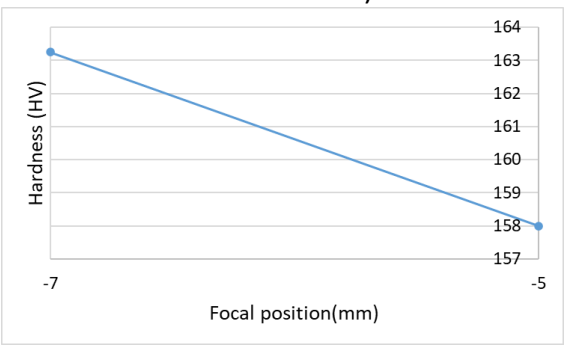
The resulting factorial model enables the exploration of hardness variations in response to controlled changes in technological parameters and provides a foundation for optimizing the cutting process in high-reliability industrial applications.





a) Effect of laser power on hardness

b) Effect of cutting speed on hardness



c) Effect of focal position on hardness

Figure 4. Main effects of process parameters on hardness

Table 1. Experimental data

Design point	Laser power , P (W)	Cutting speed, v (mm/min )	Focal position , f (mm)	Hardnes s (HV)
1	4600	2100	-7	170
19	4800	2100	-7	159
3	4600	2300	-7	165
21	4800	2300	-7	159
7	4600	2100	-5	158
25	4800	2100	-5	150
9	4600	2300	-5	162
27	4800	2300	-5	162

#### 4. RESULTS AND DISCUSSION

This subsection analyses the main effects of the three technological factors, laser power, cutting speed, and focal position, on the hardness of X10AlCr18 steel, using a 2³ factorial design. Hardness was considered a key indicator of the quality of the resulting parts, given the potential structural changes induced by thermal energy in the HAZ.

Based on experimental observations, it is evident that laser power significantly influences material hardness, as shown in Figure 4a, where an increase in power from

4600 W to 4800 W leads to a decrease in hardness from 164 HV to 157 HV. This behaviour suggests that higher energy input promotes annealing and thermal softening of the local microstructure. Regarding cutting speed, Figure 4b shows that as the speed increases from 2100 mm/min to 2300 mm/min, hardness slightly increases from 159 HV to 162 HV. This is due to the reduced interaction time between the laser beam and the material, which limits thermal diffusion and the extension of the HAZ. In Figure 4c, modifying the focal position from -7 mm to -5 mm results in a decrease in hardness from 164 HV to 158 HV, suggesting that focusing closer to the material surface leads to a broader energy distribution in depth, which promotes extended melting and reduces local hardness.

The graphical interpretation of these relationships uses a Cartesian coordinate system, where the Ox axis represents each technological parameter, and the Oy axis indicates the measured hardness values. Comparing the slopes of the three graphs highlights that laser power has the greatest influence on hardness, followed by focal position and cutting speed.

The results suggest that maximum hardness can be achieved when the ratio between laser power and cutting speed (P/v) is minimized. In this case, a value of Pmin/vmax = 2 determines the optimal conditions for preserving the mechanical properties of the material.

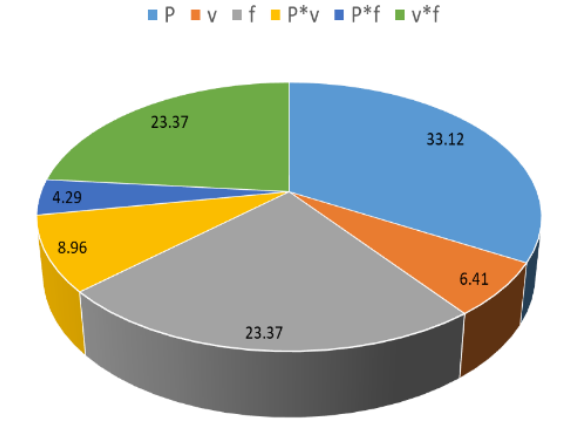
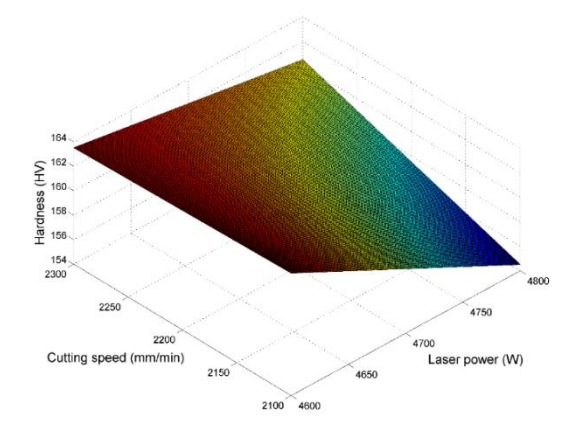
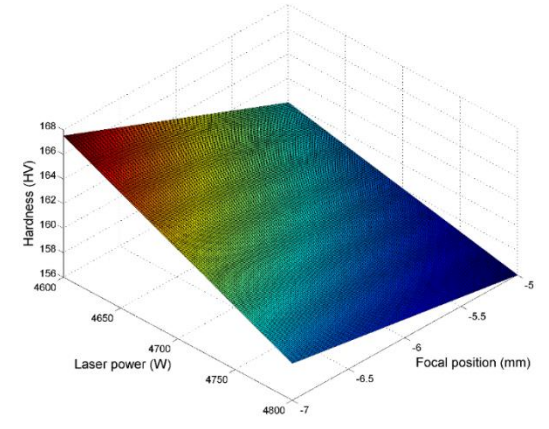


**Figure 5.** Contribution of model terms to hardness

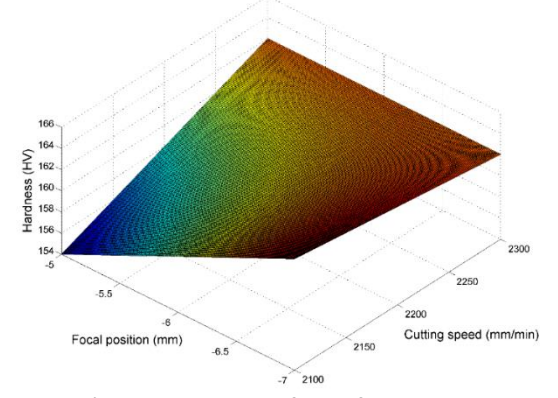
Figure 5 summarizes the percentage



 a) Interaction effect of laser power and cutting speed (for focal position of f=-6 mm)



 b) Interaction effect of laser power and focal position (for cutting speed of v=2200 mm/min)



c) Interaction effect of cutting speed and focal position (for laser power of P=4700 W)

**Figure 6.** Effects of laser cutting parameters on material hardness

contribution of each term within the statistical model.

According to the results, laser power (P) has the highest influence on hardness, accounting for 33.12%, followed by focal position (f) and the interaction between cutting speed and focal position (v\*f), each contributing 23.37%. In contrast, the interactions P\*f and P\*v had a reduced impact, and cutting speed (v) on its own contributed only 6.41% to the variability in hardness.

The 3D chart in Figure 5 provides an intuitive visual representation of each factor's in explaining the experimental response. Each sector is distinctly coloured to highlight the influence intensity of each their combinations. predictor or This representation facilitates the quick identification of critical parameters in the laser cutting process, emphasizing that hardness optimization is primarily determined by the delivered energy and the geometry of the focused beam.

For the qualitative and quantitative evaluation of the main and interaction effects of the process parameters, the following quasi-linear regression model was developed for hardness prediction:

Hardness=1278-0.32125\*P-0.5925\*v-113.25\*f+ 0.0001625\*P\*v+0.01125\*P\*f+0.02625\*v\*f

The model presents a coefficient of determination R<sup>2</sup> of 99.52%, an adjusted R<sup>2</sup> of 96.66%, and a predicted R<sup>2</sup> of 69.48%.

These values indicate a strong predictive capability of the model and a solid correlation between the estimated and experimental values.

The regression coefficient analysis enabled the ranking of each predictor's influence. Among the processed parameters, laser power exerts the strongest effect on hardness, followed by the interaction between cutting speed and focal position. The coefficients associated with the interaction terms are subunitary, suggesting moderate but significant effects. The negative sign of the laser power coefficient confirms an inverse relationship with hardness, indicating a decrease in hardness at higher power levels,

most likely due to thermal effects in the HAZ.

The developed model is graphically represented in Figure 6, where three surface plots illustrate the bidirectional interaction effects between parameters. These graphs were constructed using the RSM, keeping one parameter constant while varying the other two. The resulting surfaces highlight the combined impact of parameters on hardness, with differences in slope and contour reflecting the response sensitivity depending on the cutting regime. Broad zones with pronounced variations indicate factor pairs with significant influence, an essential aspect for process optimization and property control of the material.

The quasi-linear graphs presented were developed using RSM to highlight the combined effects of technological parameters on hardness. The resulting three-dimensional surfaces illustrate hardness variations in a colour spectrum, where chromatic gradients reflect the value levels of the response. The morphology of these surfaces, ranging from uniform planes slightly distorted to geometries, suggests a different dependence of hardness on each parameter pair. Areas with wide extension and significant variation in the response indicate strong interactions between predictors, emphasizing importance of these combinations controlling the properties of the processed material.

The results align with previous studies from the literature. For instance, Li (2021) applied the RSM methodology to optimize fiber laser cutting parameters for duplex stainless steel, a material characterized by superior thermophysical properties due to its high chromium and molybdenum content [14]. According to the author's conclusions, laser power exerts the greatest influence on the thermal distribution near the kerf edge, and a focal length of 0.4 mm, associated with maximum energy density, led to minimal surface roughness. However, excessive laser power values (>900 W) can generate defects such as slag and cavities, compromising the

quality of the cut surface. In a recent study, Liao et al. (2024) investigated high-power laser cutting (10 kW) applied to 20CrNiMo steel without the use of assist gas [15]. The authors demonstrated that both cutting speed and focal position have a direct impact on cut quality and the efficiency of slag ejection from the kerf.

#### 5. CONCLUSION

This study analysed the influence of highpower laser cutting process parameters, beam power, cutting speed, and focal position, on the hardness of X10AlCr180 steel, using a linear regression model with interaction terms, supplemented by graphical representations generated through Response Surface Methodology (RSM).

The main results can be summarized as follows:

- The generated response surfaces highlighted significant relationships between hardness and each of the analysed parameters. Each graph illustrated a sloped plane, where the angle reflects the sensitivity of hardness to changes in process parameters.
- Bidirectional interactions between parameter pairs (power–speed, power–focal position, speed–focal position) were represented by 3D surfaces that revealed nonlinear behaviours and favourable operating regimes for optimizing hardness.
- The proposed mathematical model allows the identification of optimal parameter configurations based on application-specific requirements, thus facilitating the fine adjustment of laser equipment to achieve superior performance.
- Hardness prediction proved to be an effective tool not only due to the accuracy of the estimates obtained but also due to its ability to provide an intuitive visualization of hardness variations in relation to operational parameters.
- The maximum hardness value was achieved under conditions of minimum laser power and minimum focal position, while the

lowest hardness was associated with low cutting speed and a maximum focal position.

From an energy standpoint, operating the laser at minimum power is more economical, and the influence of focal position on cutting quality is essential, a focus near the lower edge of the part leads to cleaner and more precise cuts.

Future research directions:

- Extending experiments to other types of advanced or heat-treated materials to generalize and validate the proposed model.
- Integrating additional parameters such as assist gas pressure and type, optical characteristics of the lens, or laser pulse frequency into predictive models.
- Using nonlinear prediction models (neural networks, higher-order polynomial regressions, fuzzy systems) to more accurately capture local hardness behaviour.
- Correlating hardness values with advanced microstructural analyses to substantiate the link between local structural changes and the applied technological parameters.

By deepening these research directions, future studies can contribute to increasing the efficiency, quality, and sustainability of high-power industrial laser cutting processes.

#### **REFERENCES**

- [1] M. Safari, S. M. Abtahi, and J. Joudaki, Experimental modeling, statistical analysis, and optimization of the laser-cutting process of Hardox 400 steel, *Materials*, vol. 17, no. 12, p. 2798, 2024.
- [2] M. Yurdakul, T. Tukel, and Y. T. Iç, Development of a goal programming model based on response surface and analytic hierarchy process approaches for laser cutting process optimization, *Journal of Advanced Manufacturing Systems*, vol. 21, pp. 293–316, 2022.
- [3] A. R. Patel and S. N. Bhavsar, Laser machining of die steel (EN-31): An experimental approach to optimise process parameters using response surface methodology, *International Journal of Automotive and Mechanical Engineering*, vol. 18, no. 1, pp.

- 8563-8576, 2021.
- [4] K. Sket, D. Potocnik, L. Berus, et al., Optimizing laser cutting of stainless steel using Latin hypercube sampling and neural networks, Optics and Laser Technology, vol. 182, p. 112220, 2025.
- [5] D. Itner, M. Nießen, and G. Vossen, Mathematical modeling and stability analysis for laser cutting via asymptotic expansion, *International Journal of Mechanical Sciences*, vol. 219, p. 107062, 2022.
- [6] D. Halliday and R. Resnick, *Physics*, vol. I, Bucharest, Romania: Didactic and Pedagogical Publishing House, 1975.
- [7] Y. A. Turkkan, M. Aslan, A. Tarkan, Ö. Aslan, C. Yuce, and N. Yavuz, Multi-objective optimization of fiber laser cutting of stainless-steel plates using Taguchi-based grey relational analysis, *Metals*, vol. 13, no. 1, p. 132, 2023. https://doi.org/10.3390/met13010132
- [8] D. Y. Pimenov, L. F. Berti, G. Pintaude, G. X. Peres, Y. Chaurasia, N. Khanna, and K. Giasin, Influence of selective laser melting process parameters on the surface integrity of difficult-to-cut alloys: Comprehensive review and future prospects, *International Journal of Advanced Manufacturing Technology*, vol. 127, pp. 1071–1102, 2023. https://doi.org/10.1007/s00170-023-11541-8
- [9] P. Zuo, T. Liu, F. Li, G. Wang, K. Zhang, X. Li, W. Han, H. Tian, and D. Zhu, Research progress on laser processing of carbon fiber composite materials, *Polymer Composites*, 2024. <a href="https://doi.org/10.1002/pc.29287">https://doi.org/10.1002/pc.29287</a>
- [10] C. Balasubramaniyan and K. Rajkumar, Identification of parametric conditions and the influence of laser interaction on the material removal and surface characteristics of 904L super austenitic stainless steel,

- International Journal on Interactive Design and Manufacturing, vol. 19, pp. 3527–3539, 2025.
- [11] M. Alsaadawy, M. Dewidar, A. Said, I. Maher, and T. A. Shehabeldeen, A comprehensive review of studying the influence of laser cutting parameters on surface and kerf quality of metals, *International Journal of Advanced Manufacturing Technology*, vol. 130, pp. 1039–1074, 2024.
- [12] A. K. Basak, K. Lightbody, and A. Pramanik, The effect of material intrinsic properties on the quality of machined surface during laser beam cutting, *Materials Chemistry and Physics*, vol. 336, p. 130546, 2025. <a href="https://doi.org/10.1016/j.matchemphys.202">https://doi.org/10.1016/j.matchemphys.202</a> 5.130546
- [13] A. Mahrle, M. Borkmann, and P. Pfohl, Factorial analysis of fiber laser fusion cutting of AISI 304 stainless steel: Evaluation of effects on process performance, kerf geometry and cut edge roughness, *Materials*, vol. 14, no. 10, p. 2669, 2021. https://doi.org/10.3390/ma14102669
- [14] M. Li, Evaluation of the effect of process parameters on the cut quality in fiber laser cutting of duplex stainless steel using response surface method (RSM), *Infrared Physics & Technology*, vol. 118, p. 103896, 2021.
  - https://doi.org/10.1016/j.infrared.2021.103 896
- [15] W. Liao, G. Wang, L. Zhong, Y. Chen, and J. Wang, Feasibility analysis and cutting process research on laser cutting medium-thick 20CrNiMo steel plates using a high-power fiber laser without assisted blowing, *Journal of Manufacturing Processes*, vol. 111, pp. 130–138, 2024. <a href="https://doi.org/10.1016/j.jmapro.2024.01.0">https://doi.org/10.1016/j.jmapro.2024.01.0</a>